Tubes, Sheets and Singularities in Fluid Dynamics 247-260
Proceedings of the IUTAM Symposium held in Zakopane, Poland, 2-7 September 2001.
Edited by K. Bajer and H.K. Moffatt.
FLUID MECHANICS AND ITS APPLICATIONS Volume 71
Kluwer Academic Publishers 2002
ISBN 1-4020-0980-1

A singularity-free model of the local velocity gradient and acceleration gradient structure of turbulent flow

BRIAN CANTWELL

Department of Aeronautics and Astronautics,
Stanford University
cantwell@leland.stanford.edu

Abstract Research on the fine scale structure of turbulence has led to a greatly improved understanding of the basic geometry of the local flow patterns associated with kinetic energy dissipation. One model of the local flow that has been considered previously is based on a simplification of the transport equation for the velocity gradient tensor called the Restricted Euler Equation. This equation is exactly solvable and, although the solution reproduces many of the geometrical features observed in direct numerical simulations of turbulence, the solution also exhibits a finite time singularity. It is well known that the velocity and acceleration gradients in free turbulent flows actually decrease continuously with time when measured by a Lagrangian observer. The power law in time associated with this decay can generally be estimated using dimensional analysis together with classical balances relating turbulent kinetic energy production and dissipation. This paper will describe a procedure for removing the singularity in the Restricted Euler model while maintaining the convenience of an exact solution. The resulting system is useful for generating large ensembles for statistical modeling. The new model is matched to decay rates derived from dimensional analysis and accurately predicts many of the geometrical features of both the velocity and acceleration gradient tensors. Probability density functions for both gradient fields generated by the model are compared with results from direct numerical simulation.

1. Introduction

Once the Reynolds number of a viscous flow is large enough to produce instability and once the amplitude of the instability is large enough to produce turbulence then further amplification ceases and the overall behavior of the flow tends to be independent of the viscosity. Define

u_0	–	Integral velocity scale characterizing the overall motion
δ	–	Integral length scale characterizing the overall motion

From a wide variety of experiments it is observed that the intensity of turbulence scales with the characteristic integral velocity of the flow,

$u' \approx u_0$, independent of ν. If the viscosity is decreased keeping everything else the same the rms turbulent velocity fluctuations would not be expected to change. The spectrum of turbulent fluctuations broadens as the Reynolds number is increased; the range of scales increases, but u' stays about the same and the size of the largest scale eddies stays about the same; the scale of the flow, δ tends to be independent of ν.

2. One-parameter flows

Consider the two-parameter dilation group of the Euler equations,

$$\tilde{x}^i = e^a x^i; \quad \tilde{t} = e^{a/k} t; \quad \tilde{\bar{u}}^i = e^{a(1-1/k)} \bar{u}^i;$$
$$\tilde{\tau}^{ki} = e^{a(2-2/k)} \tau^{ki}; \quad \tilde{p} = e^{a(2-2/k)} p, \tag{1}$$

where a and k are arbitrary. Note that we have invoked Reynolds number invariance in writing down the group (1) where $\tilde{\tau}^{ki}$ is stretched by the square of the factor used to stretch $\tilde{u}^i$. Furthermore all three coordinate directions are stretched by the same factor. If we act on the Reynolds equations using this group the result is

$$\frac{\partial \tilde{\bar{u}}^i}{\partial \tilde{t}} + \frac{\partial}{\partial \tilde{x}^j} \tilde{\bar{u}}^j \tilde{\bar{u}}^i + \frac{\partial \tilde{\bar{p}}}{\partial \tilde{x}^i} - \frac{\partial \tilde{\tau}^{ji}}{\partial \tilde{x}^j} =$$
$$\left(\frac{\partial \bar{u}^i}{\partial t} + \frac{\partial}{\partial x^j} \bar{u}^j \bar{u}^i + \frac{\partial \bar{p}}{\partial x^i} - \frac{\partial \tau^{ji}}{\partial x^j} \right) e^{a(1-2/k)} = 0. \tag{2}$$

The point of this is that when we remove the viscous stress term from the Reynolds equations and assume that fluctuating velocities scale with the mean, the result is a system which is invariant under the two parameter dilation group of the Euler equations rather than just the one-parameter group of the full viscous equations obtained by setting $k = 1/2$ in (1).

One-parameter flows are (usually turbulent) shear flows in open domains governed by a single global parameter with units

$$[M] = L^m T^{-n}. \tag{3}$$

Usually M is an integral invariant determined by the forces which create the flow. Following Cantwell (1981) we can use invariance under the group (1) to develop a general set of similarity rules for characterizing the space-time evolution of one-parameter flows. This is accomplished by solving the characteristic equations of (1). These are

$$\frac{dx^i}{x^i} = k \frac{dt}{t} = \left(\frac{k}{k-1} \right) \frac{du^i}{u^i} = \left(\frac{k}{2k-2} \right) \frac{dp}{p} = \left(\frac{k}{2k-2} \right) \frac{d\tau^{ki}}{\tau^{ki}}, \tag{4}$$

with integrals

$$\xi^i = \frac{x^i}{\delta(t)}; \quad P^i = \frac{u^i}{u_0(t)}; \quad P = \frac{p}{u_0(t)^2}; \quad T^{ki} = \frac{\tau^{ki}}{u_0(t)^2}, \tag{5}$$

where the time-dependent length and velocity scales are

$$\delta(t) \cong M^{1/m}(t+t_0)^k; \quad u_0(t) \cong M^{1/m}(t+t_0)^{k-1}. \tag{6}$$

The group parameter, k, is determined by the units of the governing parameter M.

$$k = \frac{n}{m} \tag{7}$$

These rules can be used to determine the temporal or spatial evolution of the flow Reynolds number

$$R_\delta = \frac{U_0}{\nu} \cong \left(\frac{M^{\frac{2}{m}}}{\nu}\right)(t+t_0)^{2k-1}. \tag{8}$$

From (8) we can see that if $k > \frac{1}{2}$ the Reynolds number increases with time and we would expect the range of scales in the flow to increase. If $k < \frac{1}{2}$ then the Reynolds number decreases with time and there is a tendency for the flow to relaminarize. If $k = \frac{1}{2}$ then the Reynolds number is constant.

3. Fine scale motions

Now let's turn our attention to the fine scales and see what we can learn about the physics of energy dissipation. This means looking closely at fluctuating strain rates and since, in a turbulent flow, the strain is closely linked to the vorticity one is eventually led to a general study of the behavior of the velocity gradient tensor. Considerations of the balance between production of turbulent kinetic energy and dissipation can be used to develop estimates for the microscale motions that are responsible for most of the dissipation of turbulent kinetic energy. The Taylor microscale, λ scales as

$$\frac{\lambda}{\delta} \approx \frac{1}{(R_\delta)^{1/2}}; \qquad \lambda \approx (\nu(t+t_0))^{1/2}. \tag{9}$$

According to (9) there is always some eddying motion in the flow with a characteristic length that varies like $\sqrt{\nu t}$ and is independent of the governing parameter M. Note that the velocity gradients of the large scale motion vary as

$$\frac{u_0}{\delta} \cong \frac{1}{t+t_0}; \qquad (t_0 > 0, \quad t > 0) \tag{10}$$

which is independent of M and ν. In a sense the large scale gradients constitute a clock which can be used to date the evolution of the flow. We can define the Kolmogorov velocity and length scales as those motions that constitute the lower limit for instability; motions with a characteristic Reynolds number of order one. This leads to the classical estimates of the Kolmogorov velocity and length scales,

$$\frac{\eta}{\delta} = \frac{1}{(R_\delta)^{\frac{3}{4}}}; \qquad \eta = \nu^{\frac{3}{4}} M^{-\frac{1}{2m}} (t+t_0)^{\left(\frac{3}{4}-\frac{1}{2}k\right)} \tag{11}$$

and

$$\frac{v}{u_0} = \frac{1}{(R_\delta)^{\frac{1}{4}}}; \qquad v = \nu^{\frac{1}{4}} M^{\frac{1}{2m}} (t+t_0)^{\left(\frac{1}{2}k-\frac{3}{4}\right)} \tag{12}$$

In a sense the Taylor and Kolmogorov microscales bracket the range of scales that can contribute significantly to kinetic energy dissipation in the flow. At scales larger than the Taylor microscale the turbulent motion is considered to be essentially inviscid. At the smallest scale are the Kolmogorov microscales with a local Reynolds number of order one. The fine scale gradients over the whole range of dissipating motions vary according to,

$$\frac{u_0}{\lambda} \approx \frac{v}{\eta} \approx \nu^{-\frac{1}{2}} M^{\frac{1}{m}} (t+t_0)^{\left(k-\frac{3}{2}\right)} \tag{13}$$

4. The inertial subrange

We can derive one of Kolmogorov's (1941) most famous results using purely dimensional reasoning and the similarity rules worked out earlier. Let's accept Kolmogorov's basic tenet and assume that a range of scales exists where the turbulent motion is independent of both ν and M and is governed only by the volumetric rate of kinetic energy dissipation. We can think of the inertial subrange as a kind of universal one-parameter flow governed by

$$M = \epsilon \approx u_0^3/\delta, \tag{14}$$

where ϵ is the turbulent kinetic energy dissipation with units $[U_0^3/\delta] = L^2T^{-3}$ and exponent $k = \frac{3}{2}$. The temporal evolution of the chaacteristic scales of the inertial subrange should follow the similarity rules in (6),

$$\delta \approx \epsilon^{1/3}(t+T_0)^{3/2}; \qquad U_0 \approx \epsilon^{1/3}(t+t_0)^{1/2} \tag{15a}$$

$$R_\delta \approx (t+t_0)^2; \qquad \lambda \approx (t+t_0)^{1/2}; \qquad \eta \approx (t+t_0)^0 \tag{15b}$$

The value $k = \frac{3}{2}$ implies very strong local forcing of the flow, typically much stronger than the forcing in most common situations. For example, to produce $k = 3/2$ at the largest scale of a jet one would need to apply

a force which increased in proportion to the fourth power of the time. We can use (15) to establish scaling laws for the turbulent kinetic energy spectrum. Assume a range of scales exists which is of order δ. Ask: how is the kinetic energy distributed among various scales? Let κ be the wave-number

$$\kappa \approx 1/\delta \tag{16}$$

The kinetic energy per unit wave-number at a given wave-number can be related to the time as follows.

$$E(\kappa) \approx \frac{u_0^2}{1/\delta} \approx \epsilon^{3/2}(t+t_0)^{5/2} \tag{17}$$

Solving for the time in (15) and substituting the reuslt into (17) produces the classical result first postulated by Kolmogorov.

$$E(\kappa) \approx \epsilon^{2/3}\kappa^{-5/3} \tag{18}$$

The $\kappa^{-5/3}$ behavior has been more or less confirmed in a wide variety of high Reynolds number experiments and so the arguments of Kolmogorov and the postulated existence of the inertial subrange are generally accepted to be correct.

5. The geometry of dissipating fine scale motion

Now let's turn our attention to a physical picture of these small scale motions. We first develop the transport equation for the velocity gradient tensor $a_j^i = \partial u^i/\partial x^j$ by taking the gradient of the Navier-Stokes equations. When the Poisson equation for the pressure is subtracted the result is

$$\frac{Da_j^i}{Dt} + a_k^i a_j^k - \tfrac{1}{3}(a_n^m a_m^n)\delta_j^i = h_j^i \tag{19}$$

where

$$h_j^i = \frac{1}{\rho}\left(\frac{\partial^2 p}{\partial x^i \partial x^j} - \frac{1}{3}\frac{\partial^2 p}{\partial x^k \partial x^k}\delta_j^i\right) + \nu\frac{\partial^2 a_j^i}{\partial x^k \partial x^k} \tag{20}$$

is the trace-free part of the acceleration gradient tensor. In the remaining sections a_j^i and h_j^i will be the main objects of interest. But before we attempt to do anything with the system of equations (19) it is natural to ask what a_j^i and h_j^i look like in a turbulent flow. For this we will turn to direct numerical simulation data. The procedure begins with a numerically-generated time-dependent flow simulation. At a given instant, the velocity gradient tensor, a_j^i is evaluated at every grid point in the computational space. The first invariant, $-a_i^i = 0$ due to incompressibility. This leaves the second and third invariants

$$Q = -\tfrac{1}{2}a_j^i a_i^j; \qquad R = -\tfrac{1}{3}a_k^i a_j^k a_i^j \tag{21}$$

as the two scalars that determine the local flow pattern at each point. The character of the eigenvalues is determined by the cubic discriminant,

$$D = Q^3 + \tfrac{27}{4}R^2. \tag{22}$$

Also of interest are the nonzero invariants of the strain and rotation tensors.

$$Q_S = -\tfrac{1}{2}s^{ij}s^{ji}; \qquad R_S = -\tfrac{1}{3}s^{ik}s^{kj}s^{ji}; \qquad Q_w = -\tfrac{1}{2}w^{ij}w^{ji} \tag{23}$$

The pdfs of the invariants contain a great deal of information concerning the geometry of the fine scales. Points near the origin correspond to low gradient values associated with the large scale motions; points far away characterize the high gradient fine scales. There is a general tendency for the (Q, R) pdf to develop a roughly elliptical shape with major axis of the ellipse aligned with the upper left and lower right quadrants. In fact the shape is really more like an inclined teardrop with the point of the teardrop lying along the $R > 0, D = 0$ branch. The strongest energy dissipating motions in the flow have a saddle-saddle unstable node geometry. This implies that the eigenvalues of the rate-of-strain tensor are ordered according to $\alpha > \beta > 0 > \gamma$. Points of high dissipation are generally characterized by high levels of vorticity, $Q_W \cong -Q_S$ although there is usually a fairly broad distribution about a 45° line in this space. At any point one can construct a locally orthogonal system of coordinates from the eigenvectors of the rate-of-strain tensor. When the vorticity vector is located relative to this system one finds, in a region of high dissipation a strong tendency for the vorticity to be aligned with the direction of the smaller of the two rate-of-strain eigenvalues.

What about the acceleration gradient tensor, h_{ij}? Cheng (1996) carried out a detailed study of this tensor using low-Reynolds number computations of homogeneous and isotropic turbulence as well as the wake computations of Sondergaard *et al.* (1996). Figure 1 shows the invariants of h computed in (Sondergaard *et al.* 1996). It appears that h^i_j looks a lot like a^i_j but with a change in sign, $h_{ij} \sim -a^i_j$. When the data is conditioned on higher and higher rates of dissipation, the invariants of h tend to gather closer and closer to the $R_h < 0, D_h = 0$ branch and for points within 75% of the maximum kinetic energy dissipation the data literally hugs the line. It appears that in regions of high dissipation, $R_h \cong -\frac{4}{27}|Q|^{3/2}$ is a good approximation. In the higher Reynolds number wake simulations of Sondergaard shown below in Figure 2 the strain invariants of h_{ij} are seen to lie closer and closer to the origin as the data is conditioned on higher and higher rates of kinetic energy dissipation. In contrast the strain invariants of a^i_j always lie far from the origin in

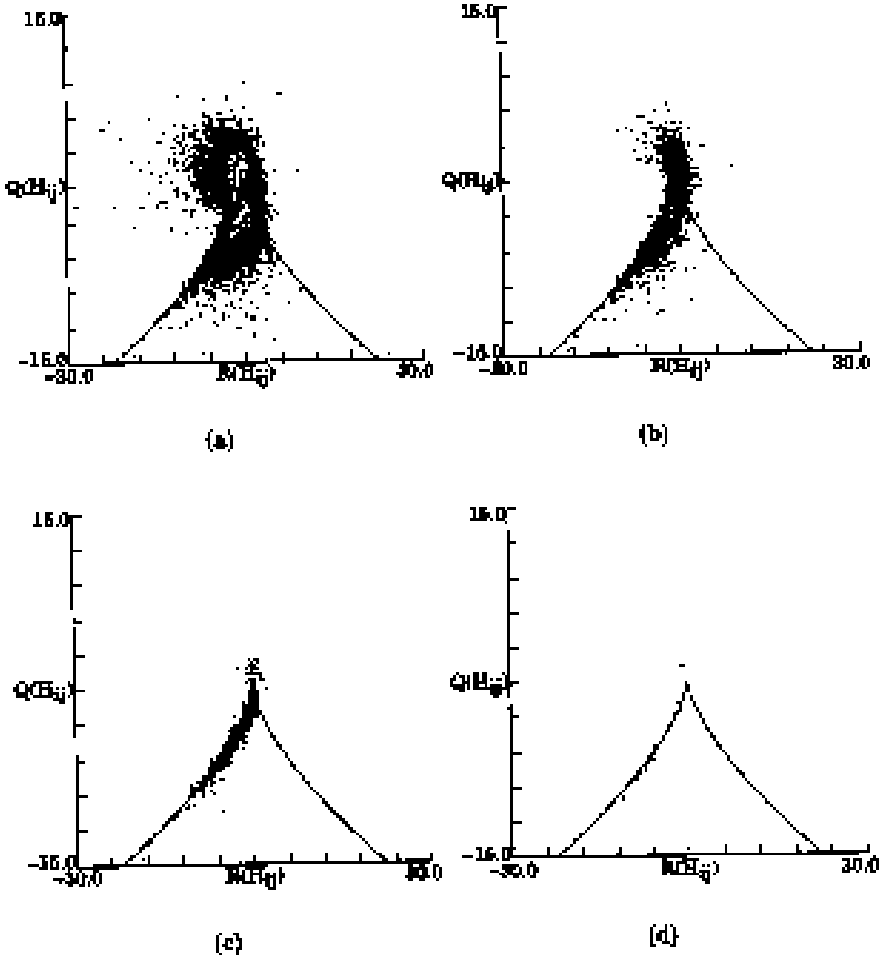

Figure 1. Logarithmic contour plots of the joint pdf of Q versus R for h_{ij} from a simulation of homogeneous and isotropic turbulence by Cheng (1996). Data conditioned at various levels of maximum local kinetic energy dissipation. (*a*) 0% (all data points), (*b*) 25%, (*c*) 50%, (*d*) 75%.

regions of high dissipation. Although the observations described above are for two specific flows, a variety of flow cases have been studied, and the basic geometry of both tensors in a region of high dissipation tends to be the same for all flows; they are universal.

Now we will attempt to develop a universal model of the small scales that reproduces the geometry of a_{ij} and h_{ij}. We begin with (19) and

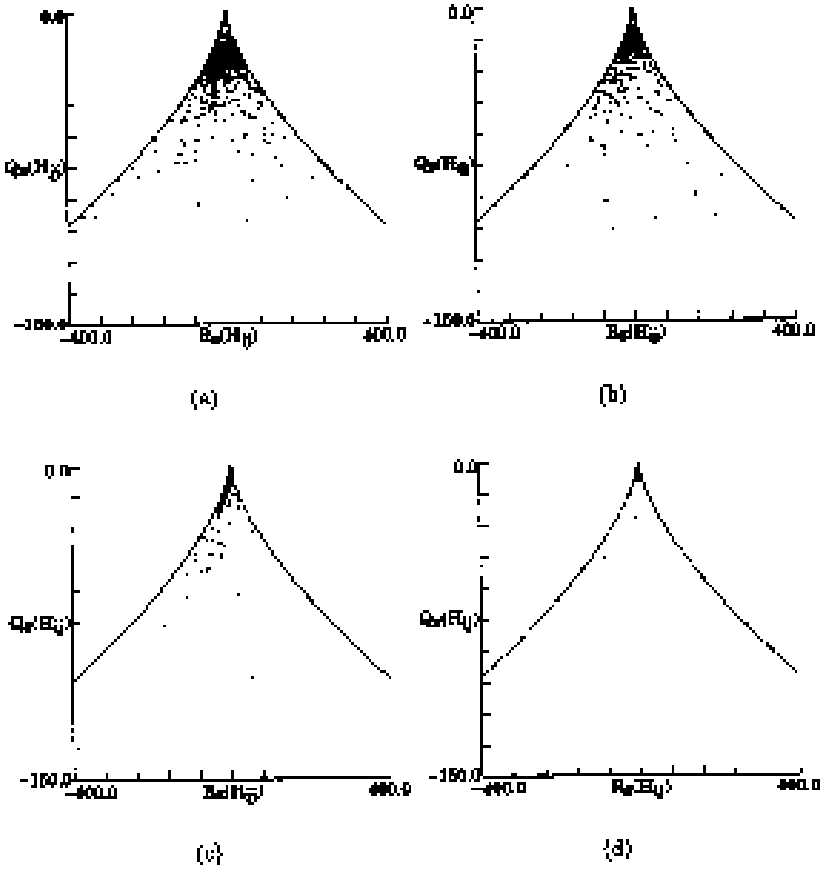

Figure 2. Logarithmic contour plots of the joint pdf of the strain invariants Q_S versus R_S for h_{ij} from a simulation of a time-developing wake by Sondergaard (1966) at a Reynolds number of 2768. Data conditioned at various levels of maximum local kinetic energy dissipation. (*a*) 0% (all data points), (*b*) 25%, (*c*) 50%, (*d*) 75%.

(20). The tensor h^i_j describes the effect of viscous diffusion and anisotropic pressure forces on the evolution of the velocity gradient tensor. It is instructive to look at the solution of the homogeneous case $h^i_j = 0$. In this cae (19) becomes a set of quadratically coupled, nonlinear ordinary differential equations for the nine components of the velocity gradient tensor called the restricted Euler equation. The cubic discriminant,

$$D = Q^3 + \tfrac{27}{4}R^2 \tag{24}$$

is conserved for all particles under this approximation. With this integral of the motion known, the time evolution of the two invariants can be determined in terms of elliptic functions. Once $Q(t)$ is known the complete system can be solved exactly for $a^i_j(t)$. The discriminant defines an appropriate time scale for normalizing all the variables in the problem, $t_{norm} = (\mathrm{abs}(D))^{1/6}$. Let

$$A^i_j = t_{norm} a^i_j; \qquad q = t^2_{norm} Q; \qquad r = t^3_{norm} R; \qquad \tau = \frac{t}{t_{norm}} \tag{25}$$

For any initial condition, the solution evolves to,

$$A^i_j = \frac{2^{1/3}}{\tau_{singular} - \tau} K^i_j; \qquad (\tau \leq \tau_{singular}) \tag{26}$$

where K^i_j satisfies the following matrix relationship

$$K^i_k K^k_j + \tfrac{1}{2^{1/3}} K^i_j - 2^{1/3} \delta^i_j = 0. \tag{27}$$

The restricted Euler system has the property that solutions become singular in finite time. To remedy this let's return to (19). Let

$$a^i_j = f(t) b^i_j \tag{28}$$

Equation (19) becomes,

$$f \frac{db^i_j}{dt} + \frac{df}{dt} b^i_j + f^2 b^i_k b^k_j - f^2 \tfrac{1}{3} (b^m_n b^n_m) \delta^i_j = h^i_j. \tag{29}$$

Here is the crucial step; assume that,

$$h^i_j = \frac{df}{dt} b^i_j \tag{30}$$

and divide (29) through by f^2. This transforms the full equation (51) to the restricted Euler but with the flexibility to define a new time. The equation becomes,

$$\frac{1}{f(t)} \frac{db^i_j}{dt} + b^i_k b^k_j - \tfrac{1}{3} (b^m_n b^n_m) \delta^i_j = 0. \tag{31}$$

Now we define the new time,

$$dt_b = f(t) dt. \tag{32}$$

This enables us to remove the singularity and continue to exploit the exact solution of the restricted Euler equation. The discriminant is used again to define a normalizing time,

$$t_{b\,norm} = (\mathrm{abs}(Q^3_{b\,initial} + \tfrac{27}{4} R^2_{b\,initial}))^{1/6}, \tag{33}$$

and let

$$B_j^i = t_{b\,norm} b_j^i; \quad q_b = t_{b\,norm}^2 Q_b; \quad r_b = t_{b\,norm}^3 R_b; \quad \tau_b = \frac{t_b}{t_{b\,norm}}. \tag{34}$$

The asymptotic behavior of the solution is

$$B_j^i = \frac{2^{1/3}}{\tau_{b\,singular} - \tau_b} K_j^i. \tag{35}$$

According to our previous discussion of fine scales the physical velocity gradient tensor should behave according to (13),

Let's require that the asymptotic behavior of the physical velocity gradient tensor is,

$$a_j^i = \nu^{-1/2} M^{1/m} (t + t_0)^{k-\frac{3}{2}} H_j^i. \tag{36}$$

Now using,

$$a_j^i = f(t) b_j^i \tag{37}$$

$$\nu^{-1/2} M^{1/m} (t + t_0)^{k-\frac{3}{2}} K_j^i = \frac{2^{1/3}}{t_{b\,norm}(\tau_{b\,singular} - \tau_b)} K_j^i f(t)$$

we can write,

$$f(t) = \frac{\nu^{-1/2} M^{1/m} (t + t_0)^{k-\frac{3}{2}}}{2^{1/3}} t_{b\,norm}(\tau_{b\,singular} - \tau_b), \tag{38}$$

or using (32),

$$\frac{d\,t_b}{(t_{b\,norm}\tau_{b\,singular} - t_b)} = \frac{\nu^{-1/2} M^{1/m} (t + t_0)^{k-\frac{3}{2}}}{2^{1/3}}\, dt. \tag{39}$$

Integrating (39) enables one to express t_b in terms of physical time t. For $k \neq \frac{1}{2}$

$$\frac{t_{b\,norm}\tau_{b\,singular} - t_b}{t_{b\,norm}\tau_{b\,singular} - t_{b\,initial}} = \exp\left(\frac{\nu^{-1/2} M^{1/m} \left[(t + t_0)^{k-\frac{1}{2}} - t_0^{k-\frac{1}{2}} \right]}{(k - \frac{1}{2}) 2^{1/2}} \right). \tag{40}$$

For $k = \frac{1}{2}$

$$\frac{t_{b\,norm}\tau_{b\,singular} - t_b}{t_{b\,norm}\tau_{b\,singular} - t_{b\,initila}} = \left(\frac{t + t_0}{t_0} \right)^{-2^{-1/3}\nu^{-1/2} M^{1/m}}. \tag{41}$$

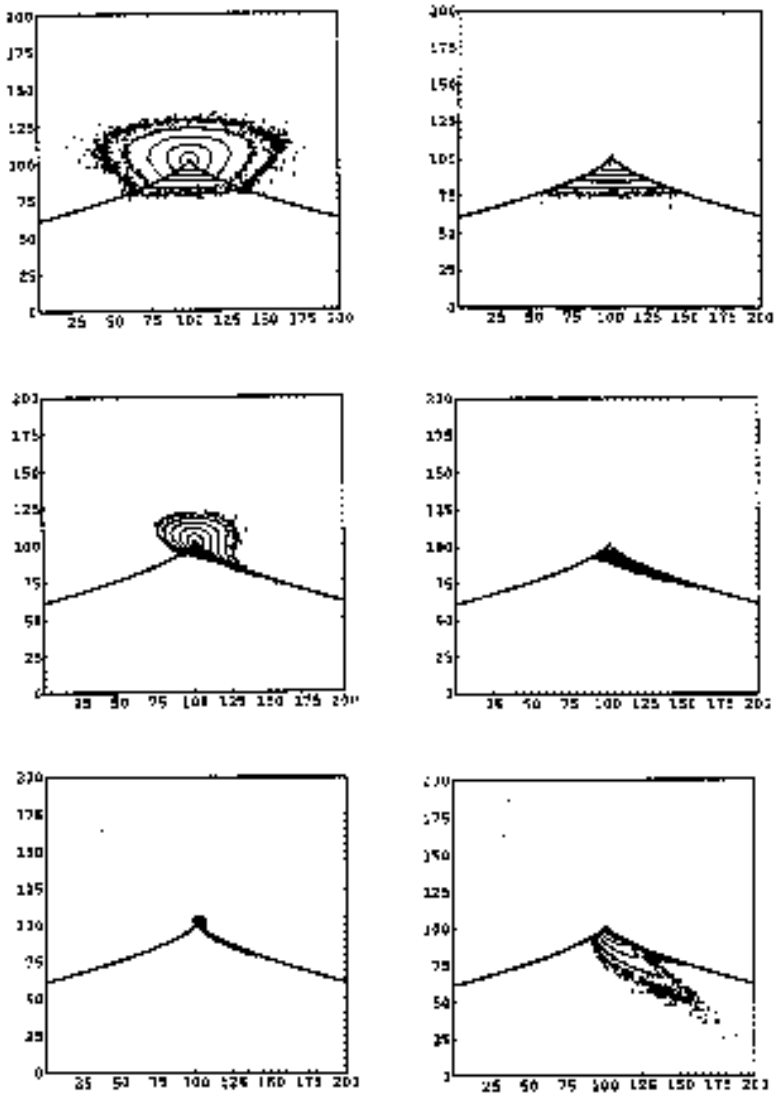

Figure 3. Time development of logarithmic contour plots of the joint pdf of Q versus R for a_{ij} (left figures) and of Q_S versus R_S (right figures) from an initially random ensemble using the Restricted Euler solution. The case shown is for $k = 3/2$.

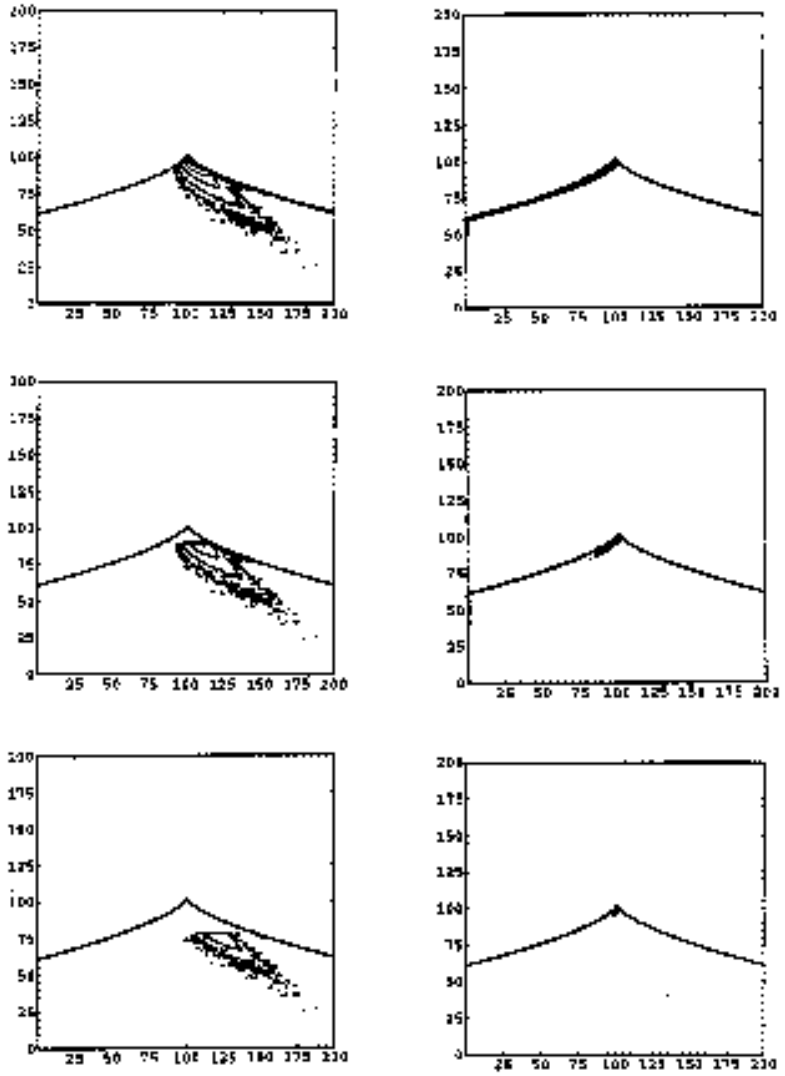

Figure 4. Logarithmic contour plots of the joint pdf of Q_S versus R_S for a_{ij} (left figures) and of Q_{hS} versus R_{hS} for h_{ij} (right figures) from an initially random ensemble using the Restricted Euler solution and the model expressed in (47). Data conditioned at various levels of maximum local kinetic energy dissipation. (top) 0% (all data points), (middle) 50%, (bottom) 75%. The case shown is for $k = 3/2$.

Now the sought after function $f(t)$ is for $k \neq \frac{1}{2}$

$$f(t) = (t_{b\,norm}\tau_{b\,singular} - t_{b\,initial})\times$$

$$\frac{\nu^{-\frac{1}{2}}M^{\frac{1}{m}}(t+t_0)^{k-\frac{3}{2}}}{2^{1/2}}\exp\left(-\frac{\nu^{-\frac{1}{2}}M^{\frac{1}{m}}\left[(t+t_0)^{k-\frac{1}{2}} - t_0^{k-\frac{1}{2}}\right]}{(k-\frac{1}{2})2^{1/3}}\right) \qquad (42)$$

and for $k = \frac{1}{2}$

$$f(t) = (t_{b\,norm}\tau_{b\,singular} - t_{b\,initial})\frac{\nu^{-\frac{1}{2}}M^{\frac{1}{m}}}{2^{1/3}t_0}\left(\frac{t+t_0}{t_0}\right)^{-2^{-1/3}\nu^{-1/2}M^{1/m}-1}. \qquad (43)$$

For any value of k

$$\frac{df}{dt} = \left(\frac{k-\frac{2}{3}}{t+t_0} - \frac{\nu^{-\frac{1}{2}}M^{\frac{1}{m}}(t+t_0)^{k-\frac{3}{2}}}{2^{1/3}}\right)f(t) \quad . \qquad (44)$$

The physical gradient tensors are related by

$$h^i_j = \frac{df}{dt}b^i_j = \frac{1}{f(t)}\frac{df}{dt}a^i_j = \left(\frac{k-\frac{2}{3}}{t+t_0} - \frac{\nu^{-\frac{1}{2}}M^{\frac{1}{m}}(t+t_0)^{k-\frac{3}{2}}}{2^{1/3}}\right)a^i_j \quad . \qquad (45)$$

The quantity

$$R_0 = \frac{M^{\frac{2}{m}}t_0^{2k-1}}{\nu} \qquad (46)$$

plays the role of an initial Reynolds number. In terms of this parameter the model becomes

$$h^i_j = \left(\frac{k-\frac{3}{2}}{1+t/t_0} - \frac{R_0^{\frac{1}{2}}}{2^{1/3}\,(1+t/t_0)^{\frac{3}{2}-k}}\right)\frac{a^i_j}{t_0} \quad . \qquad (47)$$

This completes the model. To develop an ensemble one specifies k, R_0 and an ensemble of random initial values of b^i_j subject to the continuity equation.

6. Concluding remarks

Note that for all $k \leq \frac{3}{2}$, $\frac{df}{dt} \sim -f(t)$ and for large $t + t_0$, $\left|\frac{df}{dt}\right| \ll |f(t)|$. This leads to the properties of h_{ij} observed in the simulations described above. Figure 3 shows the development of a^i_j from an initially random ensemble. Figure 4 illustrates the tendency for h^i_j to lie along the $R_h < 0$,

$D_h = 0$ branch and to have relatively small values of the invariants in regions of high dissipation. In summary the model embodied in (30), (42) and (43) culminating in (47) reproduces many of the geometrical features of the velocity gradient tensor and the trace free part of the acceleration gradient tensor observed in direct numerical simulations.

References

Cantwell, B. J. 1981 Organized motion in turbulent flow. *Ann. Rev. Fluid Mech.* **13**, 457–515.

Cheng, W. P. 1996 Study of the velocity gradient tensor in turbulent flow. Stanford University Joint Institute for Aeronautics and Acoustics Report TR 114.

Kolmogorov, A. N. 1941 The local structure of turbulence in incompressible flow for very large Reynolds number. *C. R. Acad. Sci. U.R.S.S.* **30**, 301.

Sondergaard, R., Cantwell, B. J. & Mansour, N. 1996. The effect of initial conditions on the structure and topology of temporally evolving wakes. Stanford University Joint Institute for Aeronautics and Acoustics Report TR 118.

Soria, J., Sondergaard, R., Cantwell, B. J., Chong, M. S. & Perry, A. E. 1994 A study of the fine-scale motions of incompressible time-developing mixing layers. *Phys. Fluids*, **6** (2), Pt. 2, 871–883.